Magnetic Signatures of the 15 January 2022 Hunga Tonga–Hunga Ha'apai Volcanic Eruption

N. R. Schnepf[1] [ORCID], **T. Minami[2], H. Toh[3]** [ORCID], **and M. C. Nair[4,5]**

[1]Laboratory for Atmospheric and Space Physics, University of Colorado Boulder, Boulder, CO, USA, [2]Department of Planetology, Kobe University, Kobe, Japan, [3]Data Analysis Centre for Geomagnetism and Space Magnetism, Kyoto University, Kyoto, Japan, [4]University of Colorado Boulder, Cooperative Institute for Research in Environmental Sciences, Boulder, CO, USA, [5]National Oceanic and Atmospheric Administration, National Centers for Environmental Information, Boulder, CO, USA

Abstract On 15 January 2022, at around 04:00 UTC, the submarine volcano Hunga Tonga-Hunga Ha'apai explosively erupted. We examine data from 10 Pacific Ocean geomagnetic observatories and process the data using both high pass filters and cross-wavelet analyses to enable evaluating the time-frequency characteristics of the magnetic signals across the Pacific region. At the Western Samoa observatory (API), magnetic signals of 3–8 min period, and visible in both vertical and horizontal fields, arrived at ∼04:44 UTC. The observatories at Chichijima Island (CBI) and Easter Island (IPM) both had local magnetic signatures concurrent with the eruption's water wave arrival and period ranges from, respectively, 13–93 and 5–100+ min. At CBI and IPM, the magnetic signal may be due to both the eruption's tsunami water wave and atmospheric/ionospheric sources. Our results suggest that the magnetic signatures from the eruption are identifiable and may be further separated in future studies.

Plain Language Summary On 15 January 2022, at around 04:00 UTC, the submarine volcano Hunga Tonga-Hunga Ha'apai erupted in a violent explosion. Previous studies have identified magnetic signals from earthquake-created tsunamis, however, no such studies have identified marine magnetic signals from eruption-created tsunamis. Identifying magnetic signals from different aspects of a submarine eruption can lead to a better understanding of the eruption's mechanisms, as well as potentially improve warning systems for the tsunami created by the eruption. Toward this aim, we examine data from 10 Pacific Ocean geomagnetic observatories. We processed the data using mathematical methods that enable examining the different wave components of the timeseries. We find magnetic signals likely caused by the eruption at three different Pacific island observatories (API- Western Samoa, CBI- Chichijima Island, and IPM- Easter Island).

1. Introduction

On 15 January 2022, at around 04:00 UTC, the submarine volcano Hunga Tonga-Hunga Ha'apai explosively erupted. The volcano had been erupting for the previous 24 hr, as well as intermittently in the preceding month, but the explosion that started at 04:00 UTC on 15 January was by far the largest event. The shock wave from the largest explosion of the eruption produced a sonic boom that was heard within 9 hr in Alaska, USA (9,370 km away). Tonga's islands were bombarded by tsunami waves of 2–15 m height and three Tongan people died from the tsunami so far, while many others were injured. The tsunami caused flooding, property damage, and two deaths as far away as Peru (Sennert, 2022).

Since the foundational work of Faraday (1832), physicists have known that salty water traveling through Earth's background magnetic field induces electric currents and secondary electromagnetic fields. Recently, there has been much work to study and characterize the magnetic signals from earthquake induced tsunamis (Ichihara et al., 2013; Klausner et al., 2016; Lin et al., 2021; Manoj et al., 2011; Minami et al., 2017, 2021; Schnepf et al., 2016; Sugioka et al., 2014; Tatehata et al., 2015; Toh et al., 2011; Utada et al., 2011). There are no past studies of the marine electromagnetic signals induced by volcanic eruptions. Instead, there is much literature on volcanic eruptions' atmospheric and ionospheric impacts to the point that ionospheric data has been used to provide information on the volcanic eruption (Astafyeva, 2019; Dautermann, Calais, Lognonné, & Mattioli, 2009; Dautermann, Calais, & Mattioli, 2009; Heki, 2006; Liu et al., 2017; Nakashima et al., 2016; Shults et al., 2016). As shown by Kubota et al. (2022), the Hunga Tonga-Hunga Ha'apai eruption's atmospheric acoustic

Table 1
Location of the Selected Geomagnetic Observatories

Observatory	Location	Latitude (°N)	Longitude (°E)	Altitude (m)	Nearest distance to shore (km)	Distance to eruption (km)	Water wave arrival (UTC)
API	Western Samoa	−13.807	188.225	2	0	837.6	05:12[a]
ASP[b]	Australia	−23.762	133.883	557	>900	5,218.7	
CBI	Japan	27.096	142.185	155	0.2	6,978.2	11:11
CNB	Australia	−35.320	149.360	859	101	3,810.2	
CTA	Australia	−20.090	146.264	370	108	3,996.6	
EYR	New Zealand	−43.474	172.393	102	26.3	2,786.4	
HON	United States	21.320	202.000	4	0.9	5,001.5	09:07
IPM	Easter Island	−27.171	250.580	83	1.6	6,685.6	13:42
KAK	Japan	36.232	140.186	36	34	7,831.5	
KNY	Japan	31.420	130.880	107	10.8	8,120	
MMB	Japan	43.910	144.190	42	11.8	8,240.6	
PPT	Tahiti	−17.567	210.426	357	2.5	2,733.5	06:48

Note. The volcanic eruption occurred at 184.618°E and 20.536°S.
[a]The nearest water level station to API was located ∼128 km southeast of the geomagnetic observatory. [b]marks the observatory used as the remote reference in the cross-wavelet analysis.

waves deformed the sea surface so that tsunami-like water level variations occurred hours before the actual tsunami water wave arrived. Undoubtedly, these acoustic waves also caused ionospheric disturbances.

Here we provide a comprehensive evaluation of magnetic signatures from the ∼04:00 15 January 2022 Hunga Tonga–Hunga Ha'apai volcanic eruption. We do not attempt to separate internal and external magnetic fields– the "event signal" may be from the magnetic fields induced by the tsunami water wave, by the propagation of acoustic waves in the neutral atmosphere (which then deformed the electrically conductive sea surface) or in the electrically conductive ionosphere (which directly induces its own magnetic field) (Astafyeva, 2019; Kubota et al., 2022). Instead, we analyze the time-frequency characteristics of signals at several Pacific Ocean observatories to determine whether magnetic signals are local to a given observatory or concurrent at multiple.

2. Analysis of Observatory Data

2.1. Observatory Data

Data was obtained from several International Real-time Magnetic Observatory Network (INTERMAGNET) observatories and also from a Japan Meteorological Agency (JMA) observatory (CBI) located at Chichijima Island. Table 1 specifies the locations of these observatories and Figure 1 illustrates their positions relative to the eruption site (denoted by a red star). Generic mapping tools was used to produce the map (Wessel et al., 2019).

For each of these observatories, vector data of 1 min sampling was used. The downward vertical component (Z) was used as is, but the northward (X) and eastward (Y) components were combined into one horizontal component $\left(H = \sqrt{X^2 + Y^2} \right)$.

We used observatories from a variety of locations in the Pacific Ocean. As seen in Table 1, API (Western Samoa), CBI (Chichijima Island, Japan), and HON (Honolulu, USA) were the three observatories with the closest proximity to seawater, with API having the best signal-to-noise ratio of any of the observatories since it is directly on the coast (Figure S1 in Supporting Information S1). The Chichijima station is about 200 m from the beach, however, it is at an undisturbed portion of the island. This especially contrasts with the Honolulu observatory: HON is under 1 km from seawater but between the observatory and beach are neighborhoods that likely cause significant anthropogenic noise (Figure S2 in Supporting Information S1).
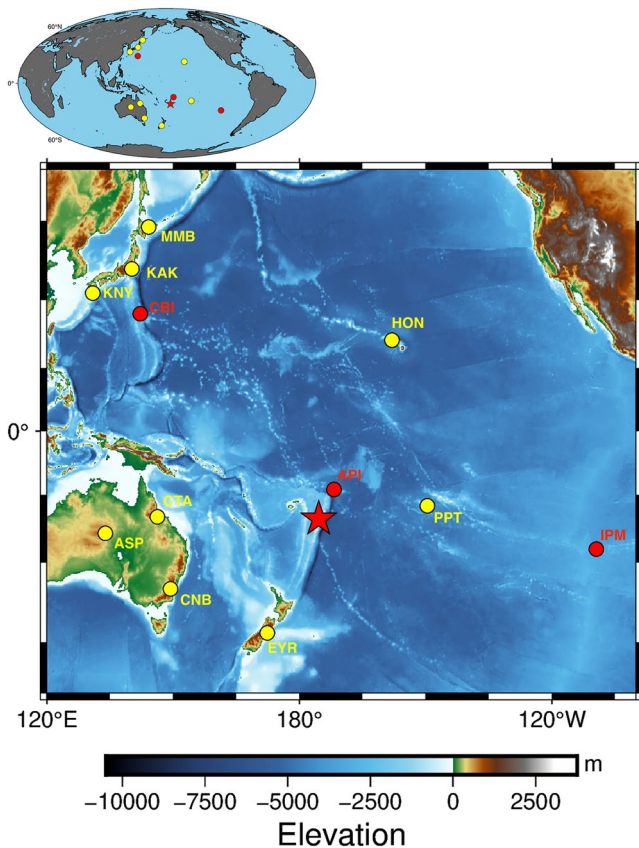
Figure 1. Map of the geomagnetic observatories (red circles for observatories with probable event signatures, yellow circles for regional observatories used in cross-wavelet analysis) used to study the magnetic signals induced by the Hunga Tonga–Hunga Ha'apai eruption. Location of the eruption is given by the red star. Generic mapping tools was used to produce the map (Wessel et al., 2019).

Closely following these three observatories, IPM (Easter Island, Chile) and PPT (Tahiti, French Polynesia) are the next two observatories closest to seawater. Similar to CBI, the Easter Island observatory is in an undisturbed portion of the island, albeit further from the coast (1.6 km vs. 200 m, Figure S3 in Supporting Information S1). Meanwhile the PPT observatory has challenges similar to HON: it is 2.5 km inland (vs. HON's 900 m) and at 357 m elevation (unlike HON's 4m altitude) with urban electromagnetic signals resting between it and the sea (Figure S4 in Supporting Information S1).

For these five island stations we obtained water wave height variation data. As discussed in the following section, the wave height data was used to determine when the eruption's water wave (due to either the atmospheric shock wave or the oceanic tsunami wave) reached the observatory. Note that for Western Samoa (API), the water level data was ∼128 km away from API on a different island. Supplementary Figure S1 in Supporting Information S1 shows their locations. Neither observatory directly faces the eruption and the water level station is in an east-facing bay that is ∼15 km further from the eruption than API. This further complicates the time lag between the water wave arrival at the geomagnetic observatory versus at the water level station.

The observatories CNB (Canberra, Australia), CTA (Charter Towers, Australia), EYR (Eyrewell, New Zealand), KAK (Kakioka, Japan), KNY (Kanoya, Japan), and MMB (Memambetsu, Japan) were selected for evaluating what time-frequency magnetic field characteristics were similar across the wider region. The observatory ASP (Alice Springs, Australia) was selected to be a remote reference station for the cross-wavelet analysis (discussed in Section 2.3) since it is deep in the Australian desert. The raw data from all of these stations are shown in Figures S5–S16 in Supporting Information S1.

### 2.2. Removing Longer Period Signals via High-Pass Filtering

The dominant variability in water level data is that due to tides. Variation in geomagnetic data is dominated by the daily fluctuations of the ionosphere–many of which are also solar synchronous. For both data sets, similar to the method of Schnepf et al. (2016), the data underwent a high pass butterworth filter. Schnepf et al. (2016), Toh et al. (2011), Manoj et al. (2011), and Utada et al. (2011) all found that tsunami magnetic signals had periods typically within 10–30 min. Ionospheric disturbances due to volcanic eruptions have been identified to have signals within a period range of 208.3–1,000 s (frequencies of 1–4.8 mHz) (Astafyeva, 2019; Dautermann, Calais, & Mattioli, 2009; Nakashima et al., 2016). Thus, we used a maximum period of 30 min so that signals with periodicities of 30 min or greater were removed. The results of this high pass filter are shown in Figures 2–4 for the observatories at, respectively, Western Samoa (API), Chichijima (CBI), and Easter Island (IPM).

The aforementioned tsunami studies were focused on those created by earthquakes. Because the volcanic eruption was a less impulsive and less discrete initiating event as compared to an earthquake, we also examined the data using a maximum period of 120 min. These results are also shown in Figures 2–4.

To determine when the eruption's water wave reached each observatory, the start of water wave height variations was selected for both sets of high pass filtered data. Note that this arriving water wave may be perturbations on the ocean surface caused by the atmospheric shock wave and the tsunami water wave's arrival may be after the initial water wave onset (Kubota et al., 2022). These arrival times are labeled on the figures.

For API, the magnetic signal appears to arrive before the water wave. However, because the water level station is on a further island from the geomagnetic observatory, the magnetic signals may in fact be concurrent with the water waves' arrival at the geomagnetic observatory.
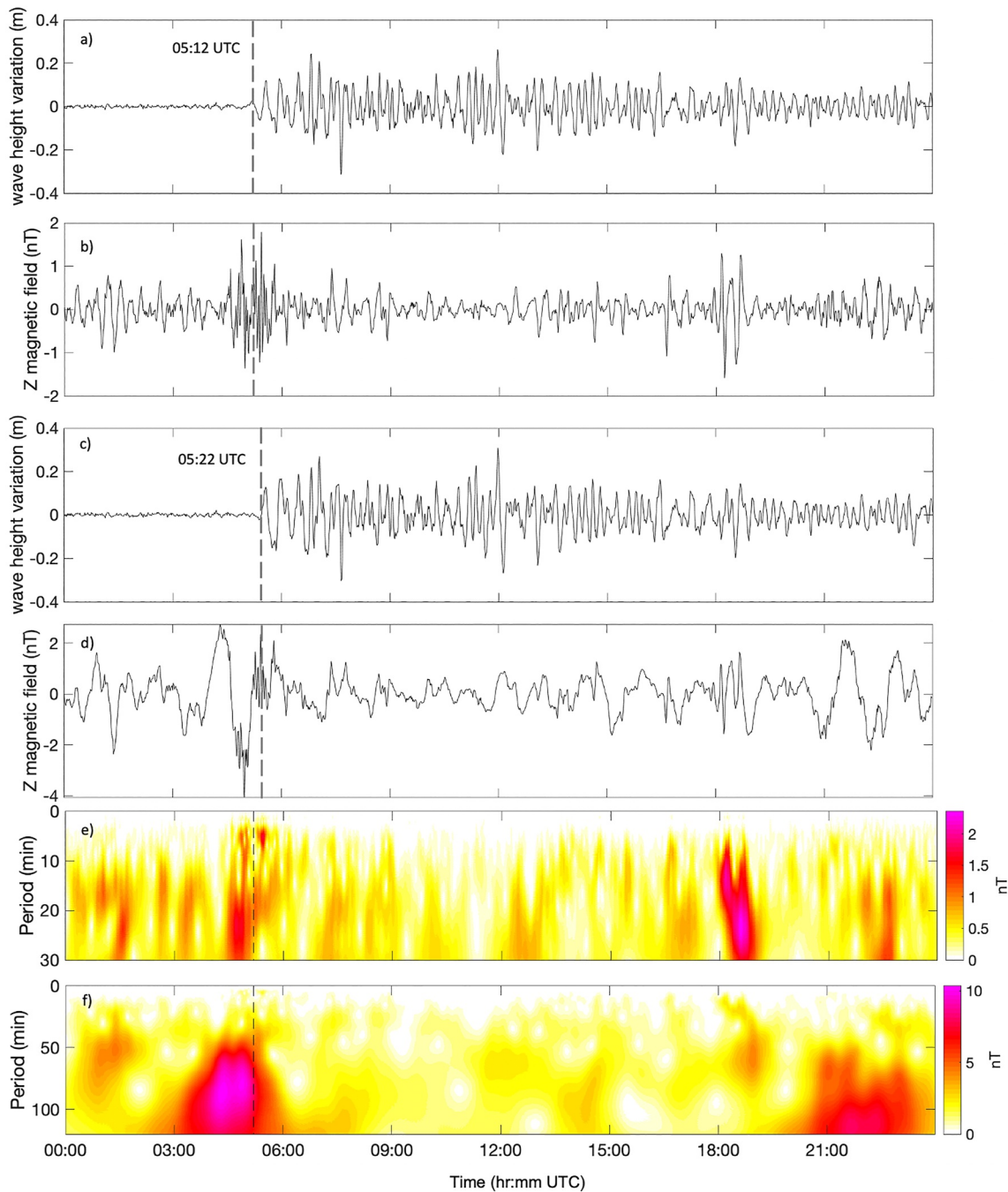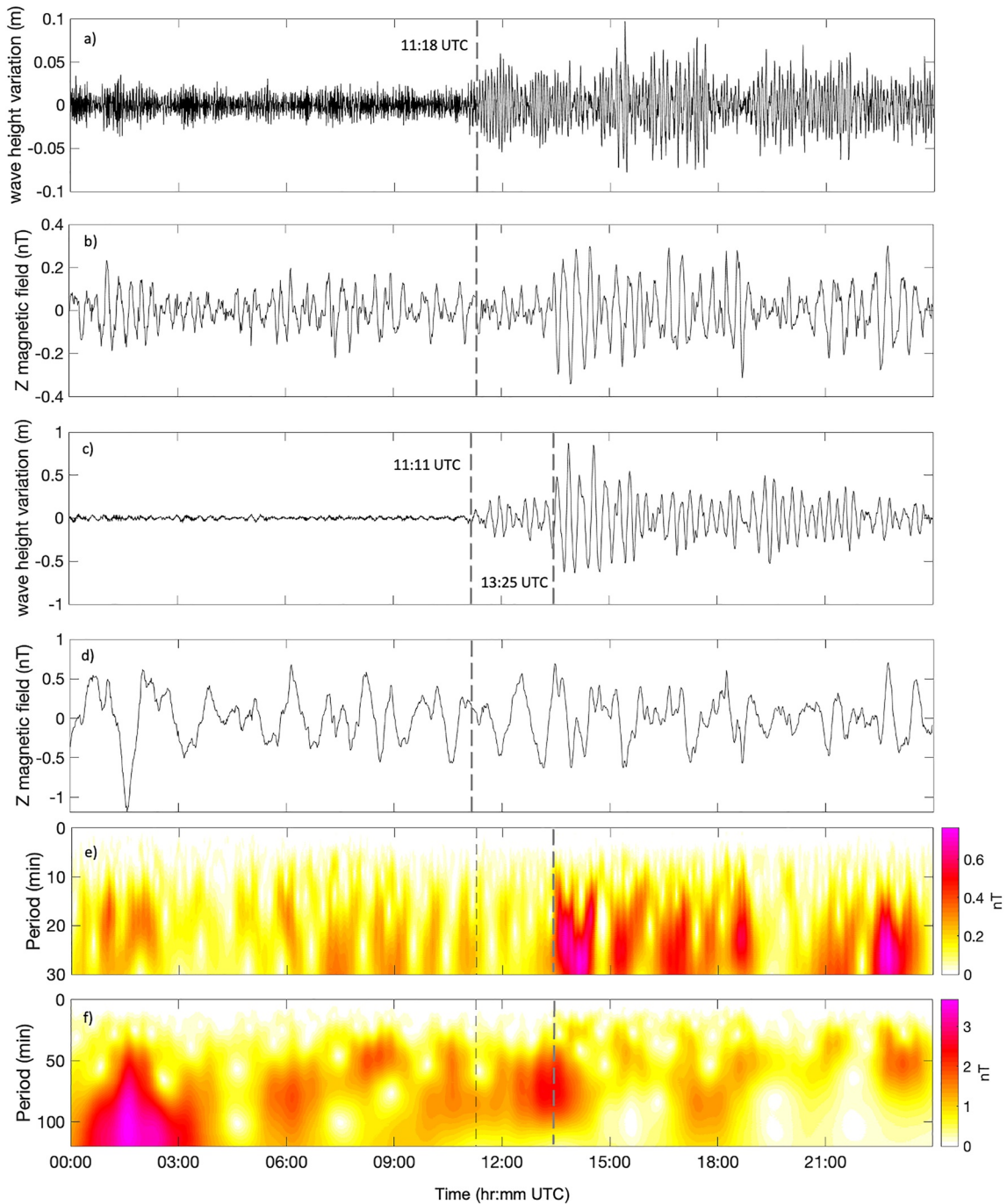
Figure 2. The water and magnetic field data for API after undergoing a high pass filter with a maximum period of 30 min (respectively, rows (a, b)) and 120 min (respectively, rows (c, d)). API's down-weighed Z wavelet matrix is shown in row (e) for a maximum period of 30 min and in row (f) for a maximum period of 120 min. For rows (e, f) the dashed line corresponds to the 05:12 UTC water wave arrival time.

2.3. Identifying Local Signals via Cross-Wavelet Analysis

To examine the time-frequency characteristics of the signals, as well as isolate the signals that are local to a given observatory, we used the cross-wavelet analysis (C-WA) methodology developed in Schnepf et al. (2016). This method performs a wavelet analysis on the horizontal and vertical magnetic field components at both a local observatory and a remote observatory. The horizontal wavelet matrices are then crossed to produce a weighing matrix so that features common to both the local and remote observatory are then down-weighed in the local vertical wavelet matrix. This weighing matrix linearly depends on the crossed amplitudes– it is best suited for

Figure 3. The water and magnetic field data for Chichijima Island (CBI) after undergoing a high pass filter with a maximum period of 30 min (respectively, rows (a, b)) and 120 min (respectively, rows (c, d)). CBI's down-weighed *Z* wavelet matrix is shown in row (e) for a maximum period of 30 min and in row (f) for a maximum period of 120 min. For rows (e, f) the first dashed line corresponds to the 11:11 UTC water wave arrival time and the second corresponds to the 13:25 UTC larger amplitude water wave arrival time seen in row (c).

geomagnetically quiet conditions. When the common external signals significantly vary in amplitude, then the weight matrix is skewed toward diminishing the common large amplitude outlier events and there can be leakage of lower amplitude common signals. This may be why the C-WA results for the Japanese observatories of KAK, KNY, and MMB show so many similar signals (Figures S17–S18 in Supporting Information S1).
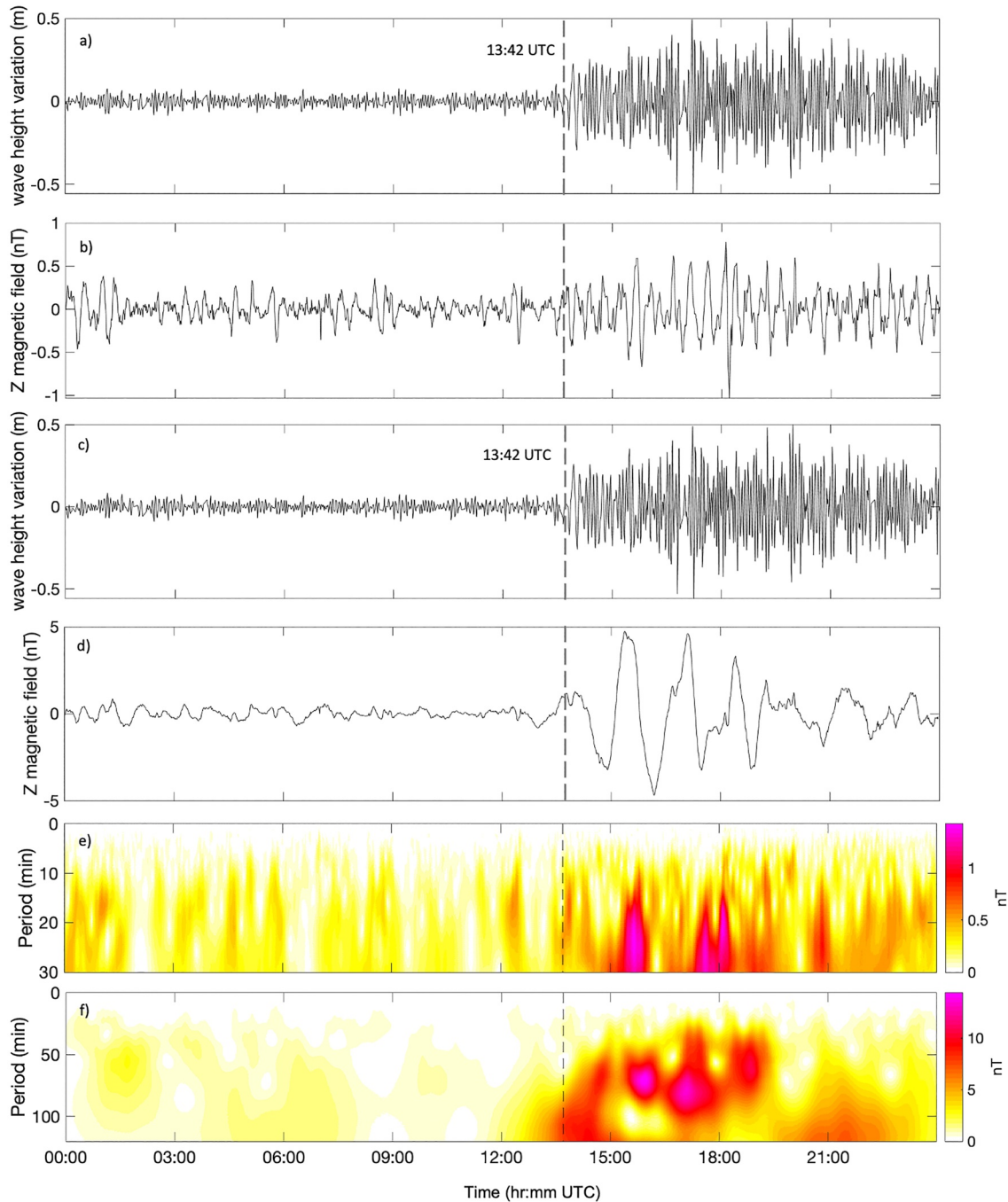
Figure 4. The water and magnetic field data for Easter Island (IPM) after undergoing a high pass filter with a maximum period of 30 min (respectively, rows (a, b)) and 120 min (respectively, rows (c, d)). IPM's down-weighed Z wavelet matrix is shown in row (e) for a maximum period of 30 min and in row (f) for a maximum period of 120 min. For rows (e, f) the dashed line corresponds to the 13:42 UTC water wave arrival time.

The wavelet and cross-wavelet analysis was performed on both the time series resulting from the $T_{max} = 30$ min and $T_{max} = 120$ min high pass filtering (high pass filtering is a pre-condition for this wavelet analysis). Figures 2–4 shows the down-weighed local vertical wavelet matrix at API, CBI, and IPM for both $T_{max} = 30$ min and $T_{max} = 120$ min. For all observatories, the cross-wavelet analysis was performed using ASP as the remote observatory. Results at all stations are presented in the Supplementary Information (Figures S17–S22 in Supporting Information S1).

3. Results and Discussion

The largest January 2022 eruption of Hunga Tonga–Hunga Ha'apai occurred at about 04:00 UTC on 15 January. This day was somewhat disturbed in terms of geomagnetic activity indices. Fortunately, most of the disturbed times were before the eruption or long after signals from the event would have reached Pacific observatories. According to the German Research Centre for Geosciences (GFZ), from 00 to 03 UTC, the planetary K (Kp) index was 5, from 03 to 09 and 12 to 18 it was a quiet index of 3, 09–12 it was an even quieter index of 2, from 18 to 21 it was 4 and from 21 to 24 it was 5 (shown in Figure S23 in Supporting Information S1).

Shown in Figure 2, the event's water wave reached Samoa by 05:12 UTC (for the $T_{max} = 30$ min high-pass filtered, HPF, data). Magnetic signals with periods of 3–8 min and strengths of ∼1–1.6 nT arrived at API starting at 04:44 UTC and persisting until 05:38 UTC. These high frequency signals were not visible at any other geomagnetic observatory in the region– none of the other considered geomagnetic observatories had magnetic signals with periods under 5 min. Interestingly, the high frequency signals were in both API's Z and H magnetic field components (Figure S9 in Supporting Information S1). Oceanic magnetic fields should only be detectable in the vertical component of coastal observatories. This suggests the signals are external in nature. Additionally, the period range of API's magnetic signature also fits with that of traveling ionospheric disturbances (TIDs) and acoustic resonance between the ground and ionosphere (Iyemori et al., 2005). This signal is most likely due to ionospheric sources and this station's close proximity to the eruption could explain why it was the only observatory with signals <5 min period. To definitively separate the sources at play here, future studies should use a combination of data sources, methods that separate external and internal magnetic fields, and perhaps numerical simulations of the expected tsunami or ionospheric signal.

At CTA, CNB, and EYR, C-WA results reveal common signals between 06 and 09 UTC for longer periods (∼15–120 min; shown in Figures S19–S20 in Supporting Information S1). In the C-WA results for $T_{max} = 30$ min, API, and CNB both have recurring signals within a period range of 15–30 min spanning from about 06 to 18 UTC. All of the observatories considered in this study, except for CTA, have recurring magnetic signals occurring after 18:00 UTC. Because 18:00 is when the Kp index became disturbed, a more rigorous study focused on external fields/sources is needed to convincingly establish whether these recurring signals are due to the eruption's atmospheric/ionospheric effects or to space weather.

Long period signals (50–120 min) at API are strongest between the time of eruption and the water wave's arrival, however, this longer period signal commences before the largest eruption, so it is unclear if this is volcano related or due to space weather. Interestingly, CTA, CNB, and EYR all have longer period signals occurring between 06 and 09 UTC, and CNB and EYR have a recurring signal within the ∼50–110 min period range. Again, further studies focused on external fields/sources would be useful for evaluating these signals.

At CBI, magnetic signals were coincident with the arrival of 1m-varying water waves (13:25 UTC, evident in Figures 3b–3c, 3e, and 3f). The dominant period range of the $T_{max} = 30$ min HPF signature is ∼13–19 min with corresponding amplitudes of 0.4–0.7 nT. For the lower frequency C-WA results (Figure 3f), the signal is smeared across the 13:25 UTC arrival time and the corresponding period range is 49–93 min with amplitudes of 1.8–2.4 nT. It is not surprising that the period range extends to ∼1.5 hr, after all, in Figure 3e there are magnetic signals recurring with roughly that periodicity.

The other Japanese observatories (KAK, KNY, and MMB) have many recurring magnetic signals throughout 15 January (Figures S17–S18 in Supporting Information S1). Considering that KAK, KNY, and MMB are all fairly inland, and how similar the signals are across the three observatories, these recurring signals must be external in origin. Determining whether these external signals are due to post-eruption ionospheric waves or a geomagnetic storm is beyond the scope of this study.

At IPM, magnetic signals were coincident with the 13:42 UTC water wave arrival (Figure 4). The high-pass filtered Z magnetic field data shows this most obviously when $T_{max} = 120$ min, however, signals are evident for both $T_{max} = 30$ and $T_{max} = 120$ min in the C-WA results (Figures 4e and 4f). Along with the initial magnetic signal, IPM has magnetic signals of 5–100 + minute periodicity coincident with the water wave and returning roughly every hour. The amplitude of the signal is greater for larger periods: it is 0.7 nT near the water wave arrival for a period of 17 min and 5–14 nT near the peaks that have periods of 60–90 min.

For both period ranges, PPT and HON do not have any magnetic signals obviously concurrent with the water wave arrival (Figures S21–S22 in Supporting Information S1). This may be due to their location: while they are on islands, both of these observatories have anthropogenic electromagnetic sources resting between them and the sea. Thus, instead of signals comparable to IPM, CBI, or API, there are recurrent signals throughout the day at HON and starting at 12:00 UTC for PPT. Some of the recurring signals appear similar to those repeating at the Japanese stations so they likely are external signals, perhaps related to the eruption or related to the Kp index increasing after 18 UTC. Either way, for T_{max} = 120 min, PPT and HON have recurring signals starting at 16:10 UTC and 16:25, respectively. This suggests that the signals at IPM occurring between the 13:42 UTC water wave arrival and ~16 UTC are truly local magnetic signatures arising from the eruption.

It is unclear whether the signals at CBI and IPM are due to the eruption's tsunami water wave, deformation of the sea surface from atmospheric acoustic waves, or ionospheric waves. Indeed, the magnetic signatures at CBI, IPM, and API likely stem from a combination of these sources.

4. Conclusions and Outlook

15 January 2022 started and ended with disturbed geomagnetic conditions but conditions were relatively quiet around the time of the Hunga Tonga–Hunga Ha'apai eruption and stayed quiet through to when oceanic and atmospheric waves from the explosion reached the various Pacific geomagnetic observatories.

The local magnetic signature at API had periods of 3–8 min and strengths of ~1 nT arrived starting at 04:44 UTC and persisting until 05:38 UTC. The high frequency signature was visible in both API's vertical and horizontal components, suggesting an ionospheric origin. However, oceanic signals could be at play here and more work is needed to definitively separate the sources.

For Chichijima Island (CBI, Japan) and Easter Island (IPM, Chile), the local magnetic signals were concurrent with the eruption's water wave arrivals. At CBI, the magnetic signatures had period bands of 13–19 min (with corresponding amplitudes of 0.4–0.7 nT) and 49–93 min (with corresponding amplitudes of 1.8–2.4 nT). Meanwhile, at IPM, we identified magnetic signatures of 5–100+ min periodicity and 5–14 nT amplitude. It is unclear whether the signals at CBI and IPM are due to the eruption's tsunami water wave, deformation of the sea surface from atmospheric acoustic waves, ionospheric waves, or combinations of all these eruption-induced sources.

The Honolulu (HON) and Tahiti (PPT) observatories lacked clear magnetic signals concurrent with their island's water wave arrival time. Instead, similar to the other more inland observatories used in this study, recurrent magnetic signals were seen for the bulk of January 15th. These signals must be external in origin, however, it is ambiguous if they are related to the Hunga Tonga–Hunga Ha'apai eruption or to Earth's space weather conditions.

Future studies should pursue methods that separate internal and external magnetic field sources at each of the near-sea observatories. Additionally, incorporating atmospheric pressure data or ionospheric total electron content data could help distinguish the different sources creating the identified magnetic signatures. Numerical studies may also shed light in separating the magnetic signal from the tsunami water wave and the ionospheric disturbances. With such future work, we believe that the magnetic signatures from submarine volcanic eruptions can be rendered sensible.

Conflict of Interest

The authors declare no conflicts of interest relevant to this study.

Data Availability Statement

With the exception of the Chichijima and Honolulu stations, magnetic field observatory data was available through INTERMAGNET (https://www.intermagnet.org/data-donnee/download-eng.php). Data from CBI at Chichijima station was obtained from the Japanese Meteorological Agency and may be accessed by contacting Kakioka Magnetic Observatory, JMA (http://www.kakioka-jma.go.jp/en/). Data from HON at Honolulu was obtained from the Kyoto World Data Centre for Geomagnetism (http://wdc.kugi.kyoto-u.ac.jp/caplot/index.html) and the station is supported/maintained by the U.S. Geological Survey. Water level data for Honolulu, USA

was obtained from the National Oceanic and Atmospheric Administration's Tides and Currents website, developed and supported by the Center for Operational Oceanographic Products and Services (CO-OPS): https://tidesandcurrents.noaa.gov/products.html. Water level data for Chichijima Island was obtained from the Japanese Meteorological Agency (contact Dr. Seiki Asari at asari@kakioka-jma.go.jp). For Western Samoa, Easter Island, and Tahiti, water level data was accessed from the Intergovernmental Oceanographic Commission's Flanders Marine Institute sea level station monitoring facility (VLIZ, 2022) and is accessible at: http://www.ioc-sealevelmonitoring.org. All of the datasets used in our study have been published online– see https://doi.org/10.25810/RPNZ-ZB30 (Schnepf, 2022). Additionally, all scripts used for data processing may be accessed at https://doi.org/10.5281/zenodo.6522947.

References

Astafyeva, E. (2019). Ionospheric detection of natural hazards. *Reviews of Geophysics*, *57*(4), 1265–1288. https://doi.org/10.1029/2019RG000668

Dautermann, T., Calais, E., Lognonné, P., & Mattioli, G. S. (2009). 12 Lithosphere—Atmosphere—ionosphere coupling after the 2003 explosive eruption of the Soufriere Hills Volcano, Montserrat. *Geophysical Journal International*, *179*(3), 1537–1546. https://doi.org/10.1111/j.1365-246X.2009.04390.x

Dautermann, T., Calais, E., & Mattioli, G. S. (2009). Global positioning system detection and energy estimation of the ionospheric wave caused by the 13 july 2003 explosion of the Soufrière Hills Volcano, Montserrat. *Journal of Geophysical Research*, *114*(B2), B02202. https://doi.org/10.1029/2008JB005722

Faraday, M. (1832). The Bakerian lecture: Experimental researches in electricity. Second series. Terrestrial magneto-electric induction. *Philosophical Transactions of the Royal Society of London*, *122*, 163–194.

Heki, K. (2006). Explosion energy of the 2004 eruption of the Asama Volcano, central Japan, inferred from ionospheric disturbances. *Geophysical Research Letters*, *33*(14), L14303. https://doi.org/10.1029/2006GL026249

Ichihara, H., Hamano, Y., Baba, K., & Kasaya, T. (2013). Tsunami source of the 2011 Tohoku earthquake detected by an ocean-bottom magnetometer. *Earth and Planetary Science Letters*, *382*, 117–124. https://doi.org/10.1016/j.epsl.2013.09.015

Iyemori, T., Nose, M., Han, D., Gao, Y., Hashizume, M., Choosakul, N., & Yang, F. (2005). Geomagnetic pulsations caused by the Sumatra earthquake on December 26, 2004. *Geophysical Research Letters*, *32*(20), L20807. https://doi.org/10.1029/2005GL024083

Klausner, V., Kherani, E. A., & Muella, M. T. A. H. (2016). Near- and far-field tsunamigenic effects on the z component of the geomagnetic field during the Japanese event, 2011. *Journal of Geophysical Research: Space Physics*, *121*(2), 1772–1779. https://doi.org/10.1002/2015JA022173

Kubota, T., Saito, T., & Nishida, K. (2022). Global fast-traveling tsunamis by atmospheric pressure waves on the 2022 Tonga eruption. Earth arXiv preprint. https://doi.org/10.31223/X5KP8M

Lin, Z., Toh, H., & Minami, T. (2021). Direct comparison of the tsunami-generated magnetic field with sea level change for the 2009 Samoa and 2010 Chile tsunamis. *Journal of Geophysical Research: Solid Earth*, *126*(11). https://doi.org/10.1029/2021JB022760

Liu, X., Zhang, Q., Shah, M., & Hong, Z. (2017). Atmospheric-ionospheric disturbances following the April 2015 Calbuco volcano from GPS and OMI observations. *Advances in Space Research*, *60*(12), 2836–2846. https://doi.org/10.1016/j.asr.2017.07.007

Manoj, C., Maus, S., & Chulliat, A. (2011). Observation of magnetic fields generated by tsunamis. *Eos, Transactions American Geophysical Union*, *92*(2), 13–14. https://doi.org/10.1029/2011EO020002

Minami, T., Schnepf, N. R., & Toh, H. (2021). Tsunami-generated magnetic fields have primary and secondary arrivals like seismic waves. *Scientific Reports*, *11*(1), 2287. https://doi.org/10.1038/s41598-021-81820-5

Minami, T., Toh, H., Ichihara, H., & Kawashima, I. (2017). Three-dimensional time domain simulation of tsunami-generated electromagnetic fields: Application to the 2011 Tohoku earthquake tsunami: Simulation of tsunami magnetic signals. *Journal of Geophysical Research: Solid Earth*, *122*(12), 9559–9579. https://doi.org/10.1002/2017JB014839

Nakashima, Y., Heki, K., Takeo, A., Cahyadi, M. N., Aditiya, A., & Yoshizawa, K. (2016). Atmospheric resonant oscillations by the 2014 eruption of the Kelud volcano, Indonesia, observed with the ionospheric total electron contents and seismic signals. *Earth and Planetary Science Letters*, *434*, 112–116. https://doi.org/10.1016/j.epsl.2015.11.029

Schnepf, N. R. (2022). *Pacific region water level variation and magnetic field data for January 15* (p. 2022). University of Colorado Boulder. https://doi.org/10.25810/RPNZ-ZB30

Schnepf, N. R., Manoj, C., An, C., Sugioka, H., & Toh, H. (2016). Time-frequency characteristics of tsunami magnetic signals from four Pacific Ocean events. In *Global tsunami science: Future Times, volume i*, (pp. 3935–3953). Springer. https://doi.org/10.1007/s00024-016-1345-5

Sennert, S. K. (Ed.). (2022). Global volcanism program, 2022, *Report on Hunga Tonga-Hunga Ha'apai (Tonga)*. Smithsonian Institution and US Geological Survey.

Shults, K., Astafyeva, E., & Adourian, S. (2016). Ionospheric detection and localization of volcano eruptions on the example of the April 2015 Calbuco events. *Journal of Geophysical Research: Space Physics*, *121*(10), 10303–10315. https://doi.org/10.1002/2016JA023382

Sugioka, H., Hamano, Y., Baba, K., Kasaya, T., Tada, N., & Suetsugu, D. (2014). Tsunami: Ocean dynamo generator. *Scientific Reports*, *4*(1), 2045–2322. https://doi.org/10.1038/srep03596

Tatehata, H., Ichihara, H., & Hamano, Y. (2015). Tsunami-induced magnetic fields detected at Chichijima Island before the arrival of the 2011 Tohoku earthquake tsunami. *Earth, Planets and Space*, *67*(1), 185. https://doi.org/10.1186/s40623-015-0347-3

Toh, H., Satake, K., Hamano, Y., Fujii, Y., & Goto, T. (2011). Tsunami signals from the 2006 and 2007 Kuril earthquakes detected at a seafloor geomagnetic observatory. *Journal of Geophysical Research*, *116*(B2), B02104. https://doi.org/10.1029/2010JB007873

Utada, H., Shimizu, H., Ogawa, T., Maeda, T., Furumura, T., Yamamoto, T., et al. (2011). Geomagnetic field changes in response to the 2011 off the Pacific coast of Tohoku earthquake and tsunami. *Earth and Planetary Science Letters*, *311*(1), 11–27. https://doi.org/10.1016/j.epsl.2011.09.036

VLIZ, F. M. I. (Ed.). (2022). *Sea level station monitoring facility*. Intergovernmental Oceanographic Commission (IOC). https://doi.org/10.14284/482

Wessel, P., Luis, J. F., Uieda, L., Scharroo, R., Wobbe, F., Smith, W. H. F., & Tian, D. (2019). The generic mapping tools version 6. *Geochemistry, Geophysics, Geosystems*, *20*(11), 5556–5564. https://doi.org/10.1029/2019GC008515